Diamond & Related Materials 74 (2017) 173–181

Contents lists available at ScienceDirect

Diamond & Related Materials

journal homepage: www.elsevier.com/locate/diamond

Depth-resolved study of hydrogen-free amorphous carbon films on stainless steel

M. Fazio [a,b,*], D. Manova [c], D. Hirsch [c], E. Valcheva [d], A. Kleiman [a,b], S. Mändl [c], A. Márquez [a,b]

[a] Universidad de Buenos Aires. Facultad de Ciencias Exactas y Naturales. Departamento de Física. Buenos Aires, Argentina
[b] CONICET- Universidad de Buenos Aires. Instituto de Física del Plasma (INFIP). Buenos Aires, Argentina
[c] Leibniz-Institut für Oberflächenmodifizierung, Permoserstr.15, 04318 Leipzig, Germany
[d] Faculty of Physics, Sofia University, Sofia, Bulgaria

ARTICLE INFO

Article history:
Received 16 December 2016
Received in revised form 7 March 2017
Accepted 11 March 2017
Available online 14 March 2017

ABSTRACT

A method to obtain depth-resolved structural information from hydrogen-free amorphous carbon films of high roughness, high thickness and grown on unpolished substrates was developed. The characterization was based on combining secondary ion mass spectrometry (SIMS) sputtering for craters at defined depth with X-ray photoelectron spectroscopy (XPS) and visible Raman spectroscopy analysis. After determination of the etching rate for the carbon film, areas with a defined end position corresponding to different known depths of the films were obtained. The SIMS etching process used did not significantly affect the structure of the amorphous carbon layer. XPS measurements of the crater bottoms provided information about the composition of the films. Visible Raman spectroscopy measurements inside of the craters were correlated with the XPS results taking into account the penetration depths of both techniques, and models aimed at predicting the sp^2/sp^3 ratio from Raman measurements were evaluated.

© 2017 Elsevier B.V. All rights reserved.

1. Introduction

For the last ten years, formation of carbon based thin films have been widely investigated due to their interesting physical and chemical properties, such as high hardness, low static and dynamic friction coefficient, optical transparency, high thermal conductivity and biocompatibility [1]. Carbon films are grown by different methods, such as chemical vapor deposition with hydrocarbon gases that lead to films with significant hydrogen content or processes that produce hydrogen free amorphous carbon films as cathodic arc evaporation using a high purity graphite cathode [1]. In general a Ti, Al or Cu interlayer is introduced between the carbon film and the substrate in order to improve adhesion. The presence of the interlayer with more compatible thermal expansion coefficient with the carbon film helps to reduce the intrinsic and interfacial stress [2].

The most frequently used methods to characterize the structure of carbon films have been visible Raman spectroscopy and X-ray photoelectron spectroscopy (XPS). Raman spectroscopy is based on the analysis of two peaks related to the sp^2 bonded sites arising near 1560 and 1360 cm^{-1} labeled as the G and D peak respectively, with the G peak associated to the stretching mode and the D peak to the breathing mode. XPS provides a direct evaluation of the sp^2 and sp^3 bonding proportion on the surface of the films. Structure depth profiles of amorphous carbon films have been limited to films of low thickness and grown on low roughness substrates such as Si. Detailed depictions of the internal film structure have been determined by X-ray reflectivity (XRR) and depth profiles on cross-section samples by electron energy loss spectroscopy (EELS) [3,4].

The growth of amorphous carbon films employing cathodic arcs with different filtering systems to remove macroparticles, ranging from S-bends to linear filters, has been extensively studied [5]. In these devices, the fraction of sp^3 bonded carbon can be controlled by applying a negative bias to the substrate which changes the energy of the impinging ions. The maximum sp^3 percentage, of approximately 85%, is found for an ion energy of 100 eV that roughly correlates to 80–100 V of negative bias depending on the characteristics of the arc and the filtering system [1]. Films with high content of sp^3 bonded sites, called tetrahedral amorphous carbon films (ta-C) presented higher hardness and higher optical gap than amorphous carbon films with high content of sp^2 bonded sites (a-C). ta-C films often feature a layering pattern where layers of low density with higher fraction of sp^2 bonds were detected. By employing cross-sectional EELS, Davis et al. identified an sp^2-rich surface layer with thickness around 1–2 nm in ta-C films

* Corresponding author at: Universidad de Buenos Aires. Facultad de Ciencias Exactas y Naturales. Departamento de Física. Buenos Aires, Argentina.
E-mail address: mfazio@df.uba.ar (M. Fazio).

http://dx.doi.org/10.1016/j.diamond.2017.03.008
0925-9635/© 2017 Elsevier B.V. All rights reserved.

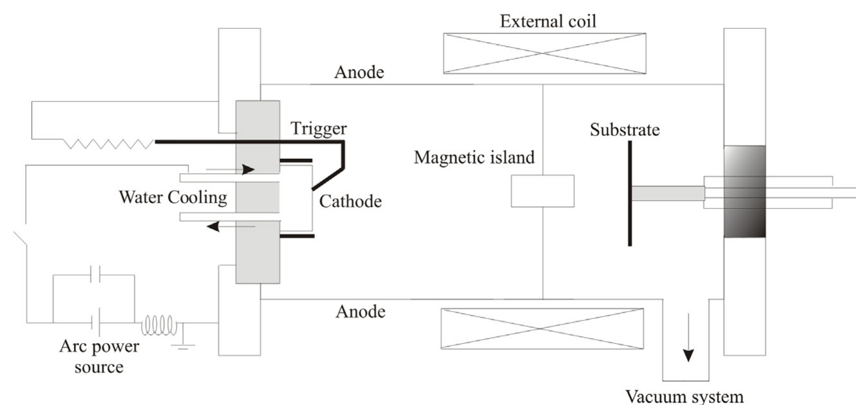

Fig. 1. Schematic view of the filtered vacuum arc system employed for production of the amorphous carbon films.

25 nm thick [6]. A low density layer near the film-substrate interface has been also found in other works on ta-C films studied by grazing-incidence XRR, cross-sectional transmission electron microscopy (TEM) and EELS [3,4,7].

Characterization of the amorphous carbon structure using Raman spectroscopy has been based on the analysis of the G and D peak in order to obtain information on the proportion of sp^2 and sp^3 bonds. Ferrari et al. proposed a three-stage model that correlates the Raman spectra of all disordered carbons to the carbon local bonding state for different excitation wavelengths [8]. The three stages of increasing disorder considered in the model are: graphite to nano-crystalline graphite, nano-crystalline graphite to a-C, and a-C to ta-C. The first stage corresponds to the reduction of the in-plane correlation length in an ordered graphite layer, the second stage represents the introduction of topological disorder with sp^3 sites ranging from 0 to 20% in a-C, and the third stage is the conversion of sp^2 sites to sp^3 sites with a percentage of 85% in ta-C. Based on experimental data from films with cross-sectional uniformity in their structure, they identified characteristic ranges of the G position and the intensity ratio between the G and D peaks (I(D)/I(G)) for each stage of the model. The authors fitted the G and D peaks with a combination of a Breit-Wigner-Fano (BWF) and a Lorentzian function, and defined the peak position as the maximum of the BWF. For an excitation wavelength of 633 nm, they found that for the third stage of the model the G position varies from 1500 cm^{-1} to 1508 cm^{-1} and I(D)/I(G) decreases from 0.2 to 0 for ta-C (where no D peak is found). Other authors have proposed fitting the G and D peaks by Gaussian functions. Schwan et al. used this fitting procedure for amorphous carbon films grown by magnetron sputtering, by previously subtracting the background of the spectra and proposing two additional peaks [9]. Tarrant et al. fitted only the Raman spectra of amorphous carbon by Gaussian functions, while proposing Lorentzian or BWF functions only for bands arising from crystallites [10].

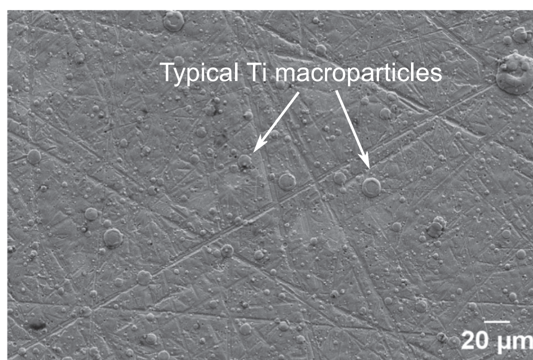

Fig. 2. Typical SEM image from the coated sample surface.

In the present work, a-C and ta-C films of approximately 1 μm thickness with a thin Ti interlayer grown on unpolished stainless steel have been studied. A method for obtaining depth-resolved structural information for the films was developed by combining oxygen SIMS sputtering with XPS and visible Raman spectroscopy analysis. The proposed method can be applied on different carbon films regardless the roughness, thickness and substrates employed, with the roughness being only a limitation on the depth resolution. XPS results were also correlated with the corresponding Raman spectra, and the different cited models aimed at predicting the sp^2/sp^3 ratio from Raman measurements were evaluated.

2. Materials and methods

The amorphous carbon films were grown by a filtered cathodic vacuum arc (filtered CVA or FCVA) system consisting of a grounded stainless steel vacuum chamber acting as anode, and a graphite cathode of 99% purity. The vacuum chamber was a cylinder of 25 cm diameter and 40 cm length with an axially centered cylindrical cathode of 8 cm diameter connected to a high power DC source (model ARCC 18 kW 150 A, ALTATEC). Both vacuum chamber and cathode were connected to a water cooling system. In Fig. 1 a schematic view of the complete FCVA device is shown. The vacuum system was comprised of a turbomolecular pump assisted by a mechanical pump reaching a base pressure lower than 10^{-4} Pa. The discharge was run at a current of 75 A. The graphitic macroparticles produced by the cathodic arc were filtered by a linear magnetic island filter, which consisted of an external coil and a permanent magnet inside the chamber producing opposing fields [11]. The permanent magnet was placed inside an aluminum jacket of 7 cm diameter and 5 cm length, and it was placed at a distance of 15 cm away from the cathode. Samples were introduced in the vacuum chamber on a water-cooled electrically insulated sample holder which was placed beyond the magnet 25 cm from the cathode.

The Ti films used as interlayers were grown by non-filtered CVA (as much less macroparticles are formed for Ti) and a detailed description of the deposition system can be found elsewhere [12]. Prior to the Ti film deposition, the substrates were cleaned in an ultrasonic acetone bath and by an Ar glow discharge plasma at 50 Pa for 60 min. The films were deposited on unpolished stainless steel 316L substrates with a surface area of 500 mm^2. The thickness of the Ti layer was 700 nm. After the Ti film deposition, the samples were introduced in the carbon FCVA system and a cleaning by Ar glow discharge plasma at 50 Pa for 30 min was carried out. Carbon films were grown with two different bias conditions: with the sample holder kept at the floating potential to obtain a-C films and with the sample holder dc biased at −100 V to deposit ta-C films. For both types of films the growth rate was estimated around 4 nm/s with thicknesses between 1.1 and 1.6 μm.

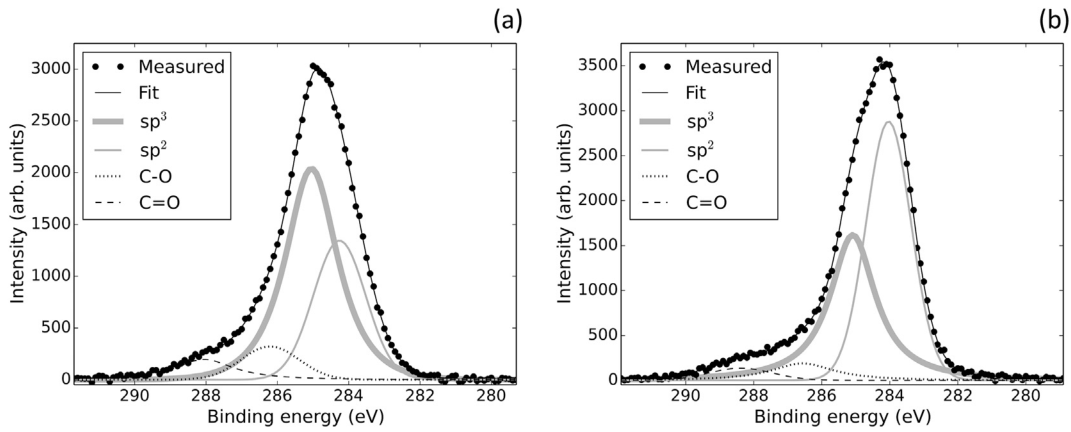

Fig. 3. XPS measurements of C 1s peak for an a-C film (a) before and (b) after the Ar^+ etching process with their corresponding fits.

The surface morphology of the coatings was studied by scanning electron microscopy (SEM) using an Ultra 55 field emission microscope (CARL ZEISS).

Secondary ion mass spectrometry (SIMS) measurements of the samples were carried out using a time-of-flight Tof-SIMS 5 (ION TOF) equipment with 15 keV Ga^+ ions for the analysis and 2 keV O_2 ions for sputter profiling. The incidence angle for both ion species was 45° at a pressure of 2×10^{-7} Pa, dominated by the oxygen gas leaking from the ion source. No sample rotation has been employed. The sputtered area was 300 μm × 300 μm and the analyzed area was 50 μm × 50 μm. The analysis beam current was about 2 Pa with the sputter beam current around 700 nA. The depth of the craters performed by SIMS was estimated by optical profilometry.

To analyze the film structure as a function of depth, several craters at different depths in the amorphous carbon film were produced by SIMS sputtering and were subsequently studied by XPS and Raman spectroscopy. The depths of interest were determined after analysis of the complete ToF SIMS measurements for each sample under study. For the new craters the chosen total area was 1000 μm × 1000 μm and the analyzed area was 500 μm × 500 μm. The selection of a larger crater area was to avoid any crater edge effects on the characterization techniques applied afterwards.

The XPS measurements were carried out using an Axis ULTRA DLD spectrometer (KRATOS), which was also equipped with an Ar^+ gun for sputtering. For selected craters, etching with 1 kV Ar^+ ions was performed and XPS measurements were taken before and after the sputtering process. The area analyzed by XPS was chosen to be a spot with 110 μm diameter. The information depths of the different photoelectron signals are limited by electron scattering processes. They should be in the range between 5 and 8 nm. Analysis of XPS measurements was performed using the commercial software Unifit 2015 (UNIFIT), which uses photoionization cross-sections and modeled information depths. The precision of the determined atomic concentrations is 1 at% for higher concentrations, for low concentrations lower. This precision could be reached by determining the instrument specific transmission function for electrons, which is involved in the Unifit program. But higher systematic errors due to concentration gradients in the analysis volume are possible.

Table 1
Calculated atomic concentrations in at% for each chemical bonding before and after the Ar^+ etching process.

Peak	Bond	Before Ar^+ etching	After Ar^+ etching
C 1s	sp^2 (at%)	26.1	47.9
C 1s	sp^3 (at%)	44.4	35.7
C 1s	C—O (at%)	6.9	5.5
C 1s	O—C=O (at%)	5.4	1.9
sp^2/sp^3		0.6	1.3

Raman spectra were recorded on a LabRAM HR 800 Visible Raman system (Horiba JobinYvon) using a 100× objective with an exposure time of 20 s. The He-Ne laser line at 632.8 nm was used as excitation source with a power of 0.5 mW. The spot size was chosen to be 1 μm in diameter and the accuracy resulted in 0.5 cm^{-1}. Based on measurements of the absorption coefficient for different amorphous carbon films [13], the penetration depth was estimated around 100 nm for the used excitation wavelength.

3. Results

Fig. 2 presents a typical SEM image from the coated sample surface. The film presents high roughness associated with the unpolished substrate surface, which is further increased by the presence of Ti macroparticles.

SIMS measurements allowed identification of the interfaces among the amorphous carbon layer, Ti layer and steel substrate. Surface contaminations including Na, K and Ca have been observed, which always present prominent signals in SIMS due to their low ionization energies. ToF SIMS measurements for both types of films show no appreciable differences. The average removal rate for amorphous carbon films was estimated around 0.09 nm/s for 1000 × 1000 $μm^2$ craters at 700 nA total current from several optical profilometry measurements. The sputter time of the carbon layer was converted into a depth-scale by using the total crater depth as determined by the estimated removal rate.

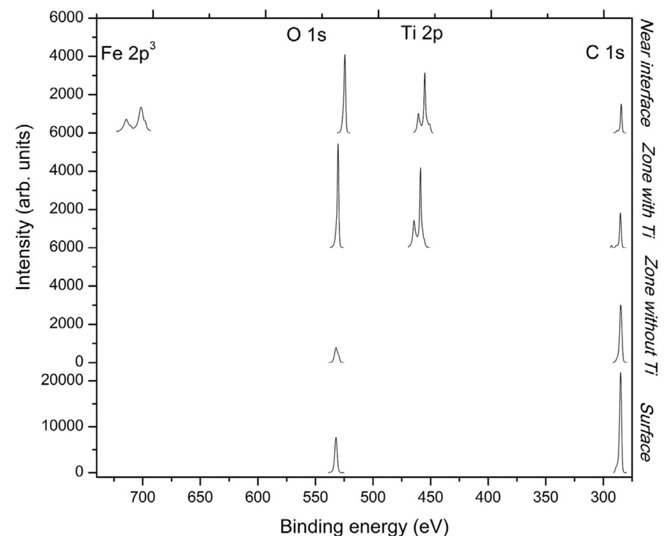

Fig. 4. Typical XPS measurements for C 1s, Ti 2p, O 1s and Fe 2p at different depths of the amorphous carbon layer.

Table 2
Average atomic concentrations in (at%) for C, O, Ti and Fe at different depths of the amorphous carbon layer.

	Surface	Zone without Ti	Zone with Ti	Near interface
C (at%)	79.9 ± 0.4	86 ± 3	25.5 ± 0.8	29 ± 2
O (at%)	14.9 ± 0.8	14 ± 3	50.7 ± 0.5	47.7 ± 0.4
Ti (at%)	0	0	23.4 ± 0.8	Up to 20.7 ± 0.1
Fe (at%)	0	0	0	Up to 17.1 ± 0.1

Nevertheless, highly selective matrix effects did not permit determination of the chemical composition of the samples from the signal intensity ratios. For both sputtering by oxygen and cesium primary ions these massive matrix effects have been observed. It is known that for polymers with increasing cross-linking a decrease of the total secondary ion yield is observed [14] while the ratio of high mass fragments to low mass fragments is also increased [15].

3.1. X-ray photoelectron spectroscopy results

For a depth-resolved analysis of the structure of the amorphous carbon film, the usual technique of XPS combined with Ar^+ sputtering was evaluated. In order to determine whether the Ar^+ sputtering affects the film structure, XPS measurements were taken before and after removing a thin layer (around 5 nm) of the amorphous carbon film by Ar^+ sputtering. Fig. 3 shows the XPS measurements of C 1s peak before and after the etching process for an a-C film. The best fit for the C1s peak in both cases was found considering contributions of the following chemical bonds: sp^2, sp^3, C—O and C═O. The calculated atomic concentrations for each chemical bonding obtained from the C 1s fit are shown in Table 1.

The sp^2 content increased from 26 at% before the sputtering to 48 at% after the process, and the sp^3 content decreased from 44 at% to 36 at%. This change in the relative bond concentrations between two craters of similar depths is too high to be associated with a variation in the film structure. Therefore, the ratio sp^2/sp^3 was strongly affected by the Ar^+ sputtering process leading to graphitization of the films. Thus this technique is not suitable for studying the structure of the amorphous carbon films as function of the depth, and subsequent analyses were carried out combining oxygen sputtering and XPS as previously described in the Experimental section. Oxygen sputtering in SIMS equipment was performed up to greater depths in the film presented in Fig. 3 and no graphitization was detected by XPS. The oxygen sputtering and intermittent exposure to air apparently do not change the sp^2/sp^3 ratio.

The composition of the bottom of different craters etched by oxygen sputtering (in SIMS device) was evaluated by XPS for both types of films. Fig. 4 shows typical XPS measurements for C 1s, Ti 2p, O 1s and Fe 2p at the surface, inside the carbon layer without the presence of Ti, inside the carbon layer with the presence of Ti and near the interface. Note that the intensity axis for XPS measurements at the surface has a different scale from the rest of the plots. The corresponding atomic concentrations for each element are presented in Table 2, with the associated errors due to the dispersion in the values obtained for different craters of similar depths.

At the surface of the films, the C content was found to be around 80 at% and the O content 15 at%. No Ti or Fe was detected. In the amorphous carbon film, zones with and without Ti macroparticles at similar depths

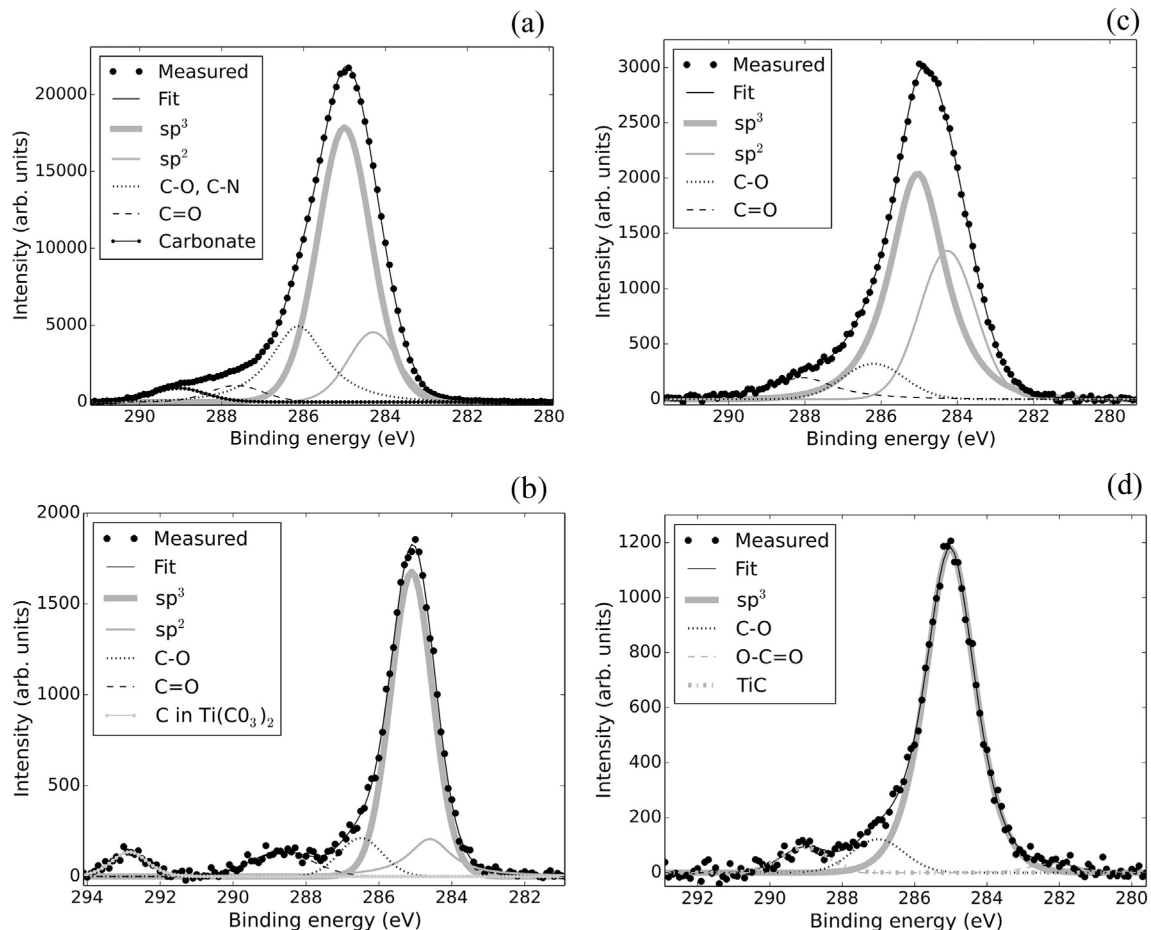

Fig. 5. Typical XPS measurements of the C 1s peak for a-C films with its corresponding fits from (a) the surface of the film, the a-C film at a depth around 30 nm (b) without Ti content and (c) with Ti content and (d) near the a-C/Ti interface. Note the different intensity scales in the plots.

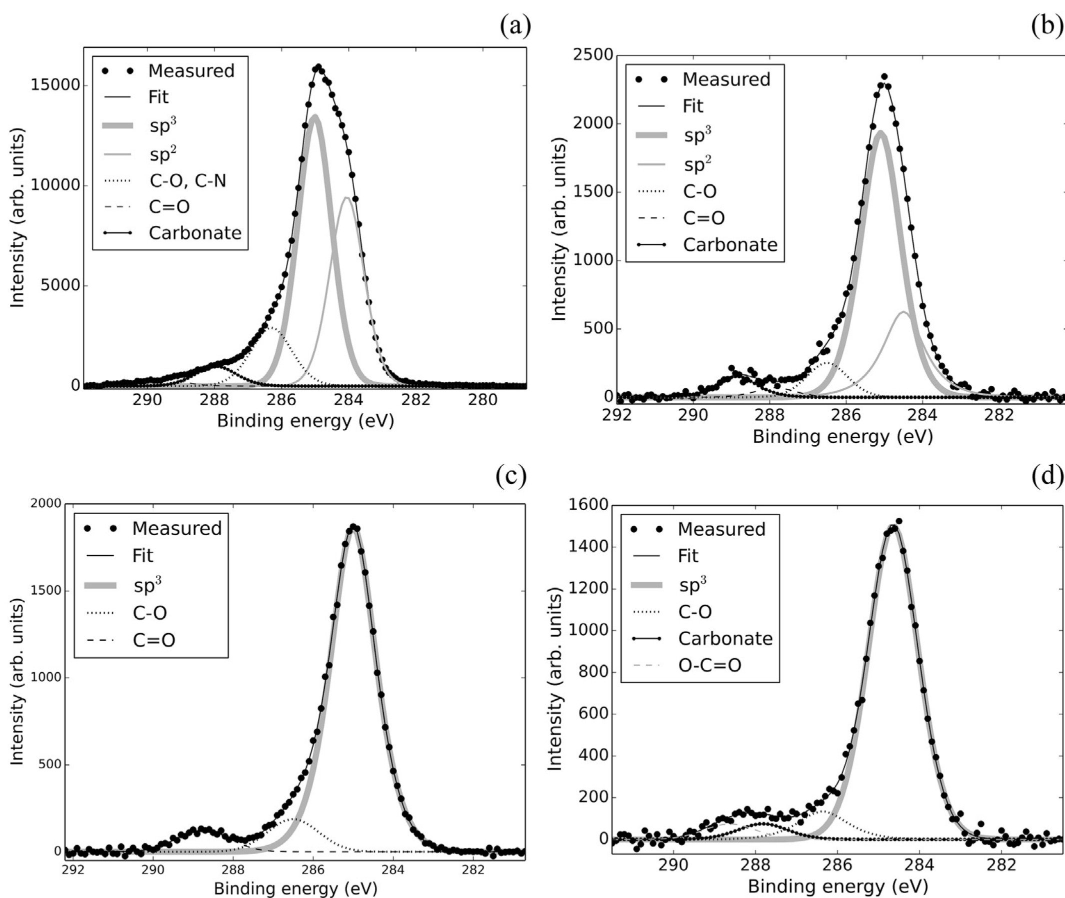

Fig. 6. Typical XPS measurements of the C 1s peak for ta-C films with its corresponding fits from (a) the surface of the film, (b) at 36 nm and (c) at 360 nm deep, and (d) near the Ti interface. Note the different intensity scales in the plots.

were identified by the Ti content. For zones with no presence of Ti, which implies no macroparticles, the C content was up to 86 at% and the O content was between 11 and 17 at%. For zones with Ti content, associated with the presence of macroparticles, the carbon content decreased to 26 at% associated with Ti content in the range of 22–25 at% (mainly associated with TiO_2) and O content up to 51%. At the

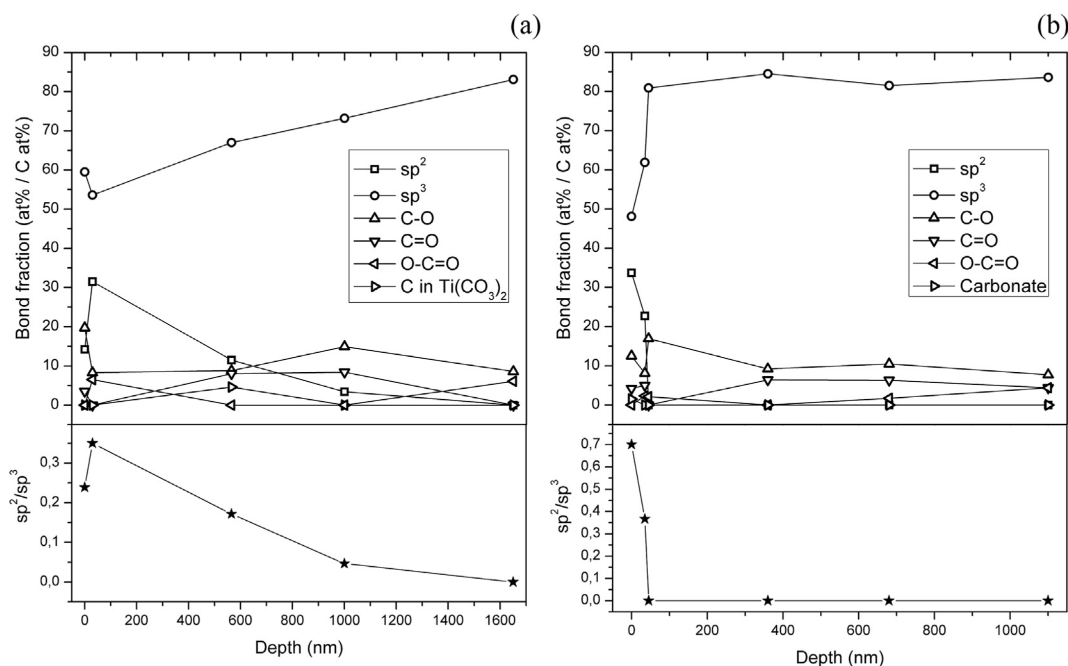

Fig. 7. Fraction of the atomic concentration of carbon bonds referred to the total carbon atomic concentration and sp^2/sp^3 ratio as function of the depth for (a) a-C and (b) ta-C films. The error bars are not distinguishable for the graph scale.

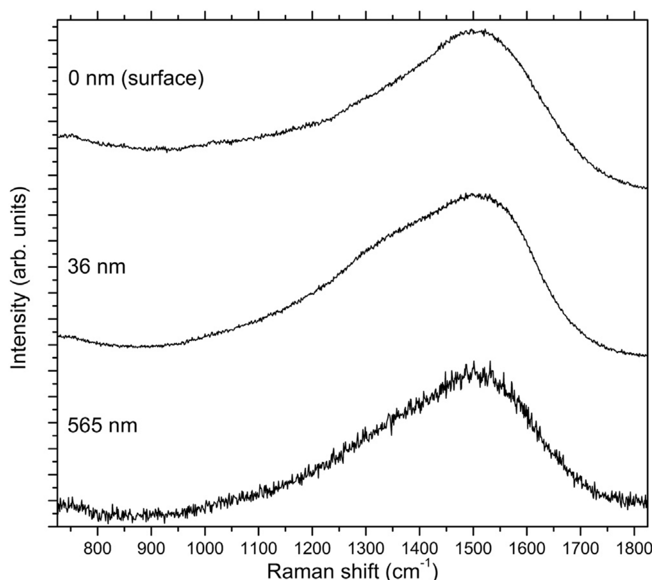

Fig. 8. Typical Raman spectra measured at the surface and at different depths of the a-C film.

amorphous carbon/Ti interface, the carbon content detected was 28–31 at%, the Ti content around 21 at% and the O content remained around 50 at%. Also concentrations up to 17 at% of Fe were found.

Fig. 5 presents typical XPS measurements of the C 1s peak for a-C films from the surface of the film, the a-C film at a depth around 30 nm without and with Ti content and near the a-C/Ti interface. The corresponding fits are also plotted in the figure. At the surface of the film, the sp^2/sp^3 ratio resulted in 0.2, with 11 at% of sp^2 bonds and 47 at% of sp^3 bonds. Also a total content around 20 at% of C—O and C═O bonds was found. In the a-C film for zones with no Ti content, the sp^2/sp^3 ratio was around 0.6 with 26 at% of sp^2 bonds and 44 at% of sp^3 bonds while for zones with macroparticles the ratio was between 0.2 and 0 with up to 3 at% of sp^2 bonds and 17–22 at% of sp^3 bonds. The content of C—O and C═O bonds was around 5 at% regardless of the macroparticle content. Near the a-C/Ti interface, no sp^2 bonds were detected with 26 at% of sp^3 bonds and content around 3 at% of C—O bonds.

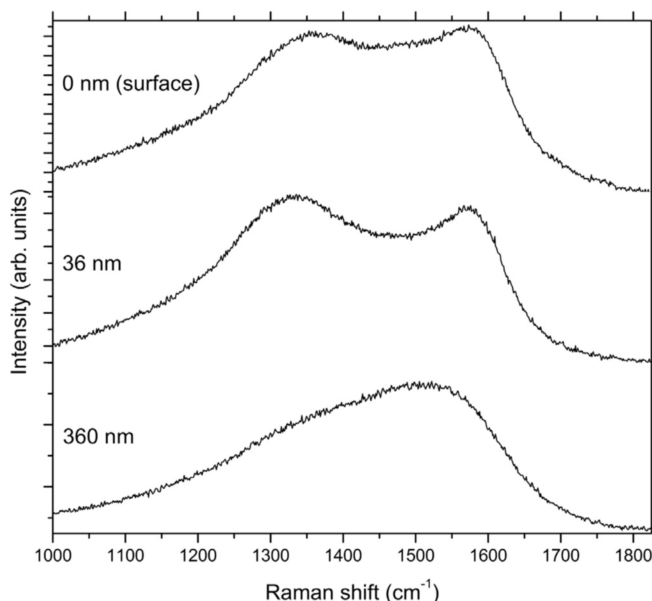

Fig. 9. Typical Raman spectra measured at the surface and at different depths of the ta-C film.

The presence of TiC was detected with concentration values around 1 at%.

Fig. 6 presents typical XPS measurements of the C 1s peak for ta-C films with its corresponding fits from the surface of the film, the ta-C film at 36 nm, at 360 nm deep, and near the Ti interface. At the surface of the film, the sp^2/sp^3 ratio resulted in 0.7, with 27 at% of sp^2 bonds and 39% of sp^3 bonds. Also a content of around 15 at% of C—O and C═O bonds was found. In the ta-C film up to a depth of 36 nm, the sp^2/sp^3 ratio was around 0.4 with 6 at% of sp^2 bonds and 16 at% of sp^3 bonds. For larger depths, however, no sp^2 bonds were detected for zones with or without macroparticles with up to 72 at% of sp^3 bonds. The content of C—O and C═O bonds was around 5 at% regardless of the macroparticle content. Near the ta-C/Ti interface, no sp^2 bonds were detected with 23 at% of sp^3 bonds and content around 2 at% of C—O bonds.

The calculation of atomic concentrations of the carbon bonds from the fit of the C 1s peak was performed for all craters at different depths. The fractions of the atomic concentration of different carbon bonds referred to the total carbon atomic concentration and the sp^2/sp^3 ratio as function of the depth for a-C and ta-C films are plotted in Fig. 7. Only bonds with atomic concentrations higher than 3 at% were included in the graphs, and for craters of similar depths the average values are presented.

3.2. Visible Raman spectroscopy results

Raman measurements were performed on the surface of the films and in craters at different depths. For craters at a depth near the amorphous carbon/Ti interface, no Raman peaks were identified due to the low carbon content in the volume probed by the technique.

Fig. 8 shows typical Raman spectra obtained from measurements at the surface and at different depths of the a-C films. The Raman spectra show no significant variations and in all cases present an asymmetric peak centered between 1508 and 1518 cm^{-1}. This is consistent with a spectrum dominated mainly by the G peak, which is associated with low sp^2/sp^3 ratios [8].

For the deeper crater, the signal-to-noise ratio decreases significantly which can be attributed to the lower carbon content in the probed volume.

Fig. 9 displays typical Raman spectra corresponding to ta-C films measured at the surface and at different depths of the ta-C layer. For the surface and depths up to 36 nm the Raman spectra present two peaks of similar intensities centered around 1360 cm^{-1} and 1570 cm^{-1}. These peaks can be associated with the D and G peak respectively, and are indicative of high sp^2/sp^3 ratios. For larger depths, the Raman spectra show a single asymmetric peak with its maximum around 1508–1510 cm^{-1} which can be identified as the G peak. This is consistent with very low sp^2/sp^3 ratios [8].

4. Discussion

ToF SIMS profiles did not feature significant differences between a-C and ta-C films, and due to matrix effects did not provide information about the chemical composition. However, these measurements allowed to identify the different layers and interfaces of the films and to correlate the O etching time with the depth for the amorphous carbon layer. Knowing the etching rate, it was possible to obtain areas with a defined end position using SIMS sputtering, corresponding to different depths of the amorphous carbon layer. Information about the structure and composition of the films was obtained from XPS measurements of the craters.

The effect of the O etching on the samples during SIMS can be evaluated from XPS measurements of the different craters for both types of films. The O content was found to increase with the etching time, from 15 at% at the surface to 50 at% near the amorphous carbon/Ti interface. However, the concentration of oxygen bonded carbon (C—O and C═O bonds) decreased from around 20 at% at the surface to 3 at% near the

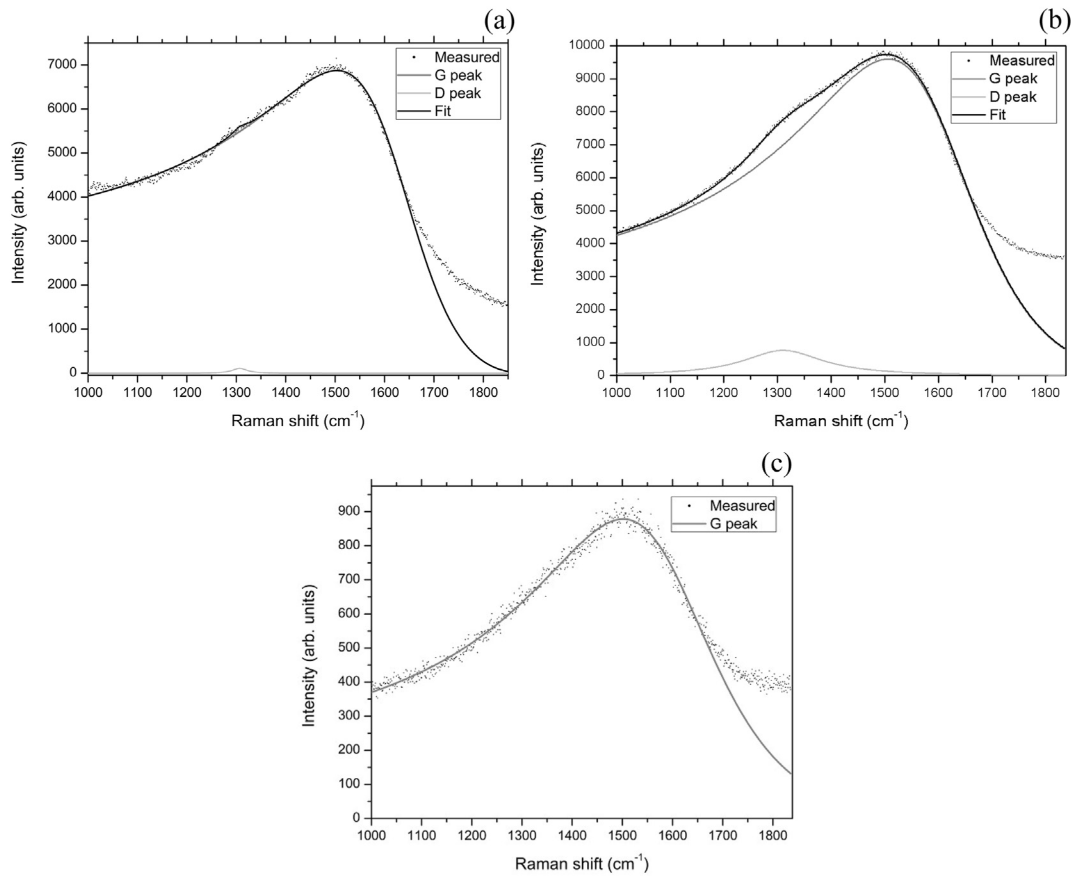

Fig. 10. Typical fit of the Raman spectra for a-C films using only BWF functions for the peaks for (a) the surface of the film, (b) at 36 nm and (c) at 565 nm deep.

amorphous carbon/Ti interface. It is possible that CO molecules formed during the etching process but they are likely to be desorbed from the surface. For etching times corresponding to depths inside the amorphous carbon layer, the highest O contents corresponded to zones with high Ti content. This correlation between O content and Ti content might be attributed to TiO_2 formation induced by the O sputtering. This effect does not seem to influence the sp^2/sp^3 ratio. Moreover, no correlation between sp^2/sp^3 ratio and the O etching time was found which indicates that the etching process does not significantly affect the amorphous carbon layer structure. Neither a monotonic increase nor a decrease of the sp^2/sp^3 ratio was observed.

a-C films presented a similar sp^2/sp^3 ratio at the surface and inside the carbon layer, varying between 0.2 and 0.6, which is consistent with the measured Raman spectra. Taking into account XPS measurements and the difference in the penetration depth of both techniques, it can be estimated that Raman is probing a volume with an average sp^2/sp^3 ratio of around 0.3. The model proposed by Ferrari et al. was applied to fit the spectra, assuming the presence of both D and G peaks which were fitted by a combination of a BWF + Lorentzian function. It was found that a BWF function alone fitted the peaks well, and the addition of a Lorentzian function did not significantly improve the fit. Fig. 10 presents the fits of the signals shown in Fig. 8, using only BWF functions for the peaks. A BWF function centered around 1310 cm^{-1} with a very low q fitted well the D peak, which indicates that the lineshape approaches a Lorentzian function. The G peak was fitted by a BWF function centered around 1500–1510 cm^{-1} and presents a marked asymmetry as indicated by a value for q around −2. The position of the D and G peaks, the intensity ratio between the peaks (I(D)/I(G)) and the coefficient of determination (c.o.d.) for the fits between 1000 and 1700 cm^{-1} and extended up to 1850 cm^{-1} are reported in Table 3. Selecting the wavelength range for the fitting around the signal maximum, from 1000 to 1700 cm^{-1}, resulting in the coefficient of determination of up to 0.987 and extending the wavelength range up to 1850 cm^{-1} the coefficient decreases less than 10%. The c.o.d. value for the range of interest was quite high and the decrease in the c.o.d. when the range was extended can be associated to the relative weight of the background compared to the G peak intensity. Background subtraction to the measured spectrum using a linear function was attempted, causing a loss of asymmetry in the signal which rendered the use of BWF functions unsuitable. The intensity ratio between

Table 3
Peak parameters from Raman spectra for craters of different depths for both types of films. The coefficients of determination (c.o.d.) calculated for the specified wavelength ranges are shown when the parameters were obtained by fitting the spectra.

Film type	Crater depth (nm)	D position (cm^{-1})	G position (cm^{-1})	Relative intensity I(D)/I(G)	c.o.d. 1000–1700 cm^{-1}/ 1000–1850 cm^{-1}
a-C	0	1307 ± 4	1505 ± 1	0.023 ± 0.005	0.992/0.906
	36	1311 ± 1	1510 ± 1	0.113 ± 0.003	0.999/0.951
	565	–	1505 ± 5	–	0.987/0.924
ta-C	0	1354 ± 1	1573 ± 1	0.98 ± 0.02	–
	36	1336 ± 1	1572 ± 1	1.04 ± 0.02	–
	360	–	1510 ± 1	–	0.996/0.922

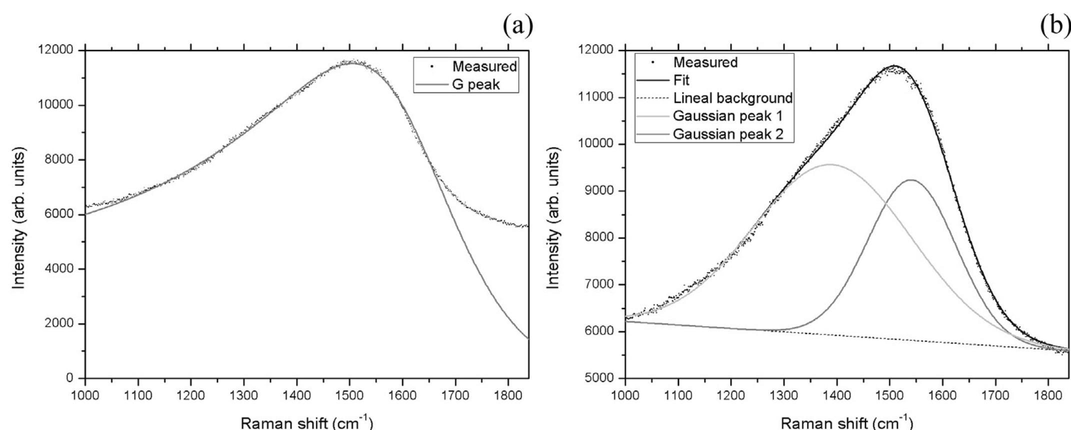

Fig. 11. Typical fits of the Raman spectra for ta-C films corresponding to craters with a depth larger than 40 nm using (a) BWF functions and (b) Gaussian functions with a linear background for the peaks.

peaks D and G was determined to be lower than 0.12 and the G peak position between 1500 and 1510 cm^{-1} for all the fits. According to Ferrari et al. and their proposed model, the measured spectra would correspond to a sample with sp^2/sp^3 ratio between 0.2 and 0.3 which is in good agreement with the ratio calculated from XPS measurements.

ta-C films feature a sp^2-rich zone up to 40 nm deep while the rest of the film has no sp^2 bonded carbon, both features being reflected in the Raman spectra for these films. Fig. 11 shows a typical Raman spectra corresponding to craters with a depth larger than 40 nm, with the spectra featuring a peak with a maximum around 1508–1510 cm^{-1} and a FWHM between 340 and 380 cm^{-1}. The model proposed by Ferrari et al. was applied, proposing again BWF functions for the D and G peak fits. The D peak intensity resulted lower than 3% of the intensity of the G peak. Therefore, it seems that the spectrum is dominated by the G peak and a good fit can be obtained with only this peak. Fig. 11a presents the fit, and the G peak position and c.o.d. are shown in Table 3. The c.o.d. value was 0.996 decreasing by 8% when the wavelength range was extended. According to Ferrari et al., the spectra should correspond to a ta-C film with a sp^2/sp^3 ratio lower than 0.18 which is in good agreement with the XPS measurements for the probed volume where no significant sp^2 bonded carbon was detected.

Another model was evaluated which is frequently used for fitting the Raman spectra [9,10] that consists of fitting by Gaussian functions. In this case, the fitting can only be done following a subtraction of the signal background due to the peak asymmetry. A linear function was proposed for the background in order to keep the model as simple as possible. Fig. 11b shows a typical fit using a linear background and two Gaussian functions. This model fits well all the range of wavelengths under study, and provides two peaks centered around 1393 and 1544 cm^{-1} respectively with similar heights. These peaks could be labeled as the D and G peaks but XPS measurements indicate there is a very low sp^2/sp^3 ratio for which no D peak (or a very low intensity D peak) is expected. This model works well because after subtracting the background, a Gaussian fit is a good choice due to the fact that the lineshape lost its asymmetry. But by subtracting the background using an arbitrarily chosen function, information of the real lineshape is lost and a false fit is obtained which does not represent the real sp^2/sp^3 ratio of the sample under study.

In the case of Raman measurements from ta-C films for the surface of the sample or at depths lower than 40 nm, the peak positions and relative intensity determined from the measured spectra are reported in Table 3. Ferrari et al. developed their model employing samples with cross-sectional uniformity. Based on XPS measurements, the Raman probed volume presents zones with pronounced differences in the sp^2/sp^3 ratio, in particular a sp^2-rich zone near the surface. Given the lack of uniformity in the film structure, an equivalent average value of the sp^2/sp^3 ratio might be expected when applying the model by Ferrari et al. However, inconsistent values of sp^2/sp^3 ratio were obtained: the G peak position corresponded to a ratio of 19 while the relative intensity indicated a ratio of 6, both significantly higher than the values found by XPS measurements for all depths. Hence, the model is not suitable for samples with large variations in the sp^2/sp^3 ratio.

5. Conclusions

Depth-resolved structural information from a-C and ta-C films with high roughness grown on stainless steel substrates has been obtained by combining SIMS sputtering with XPS and visible Raman spectroscopy analysis. The application of the proposed method can be extended to different carbon films regardless the roughness, thickness and substrates employed, with the roughness being only a limitation of the depth resolution. After determination of the etching rate for the carbon films, areas with a defined end position corresponding to different known depths of the films were obtained. The etching process used did not significantly affect the structure of the amorphous carbon layer. However, the usual etching technique of Ar^+ sputtering used for depth-resolved XPS analysis resulted in graphitization of the films. XPS measurements of the craters provided information about the structure and composition of the films. Visible Raman spectroscopy measurements of the craters where correlated with the XPS results taking into account the penetration depths of both techniques. The model proposed by Ferrari et al. was found to be suitable for estimating the sp^2/sp^3ratio from fitting the Raman spectra providing the film structure had no significant variations in the probed volume. Models based on fitting the spectra by Gaussian functions and subtracting the background have been shown to provide incorrect determinations of the sp^2/sp^3 ratio.

Acknowledgements

This work was supported by grants from Universidad de Buenos Aires (PID 20020150100103BA) and CONICET (PIP 11220120100468CO). M. Fazio acknowledges the support from the Ministerio de Educación de la República Argentina and the German Academic Exchange Service (DAAD).

References

[1] J. Robertson, Diamond-like amorphous carbon, Mater. Sci. Eng. R. Rep. 37 (4) (2002) 129–281.
[2] B. Zhou, X. Jiang, A.V. Rogachev, D. Sun, X. Zang, Growth and characteristics of diamond-like carbon films with titanium and titanium nitride functional layers by cathode arc plasma, Surf. Coat. Technol. 223 (2013) 17–23.
[3] J. Zhu, J. Han, X. Han, H.I. Schlaberg, J. Wang, sp3-rich deposition conditions and growth mechanism of tetrahedral amorphous carbon films deposited using filtered arc, J. Appl. Phys. 104 (1) (2008), 013512.

[4] A. LiBassi, A.C. Ferrari, V. Stolojan, B.K. Tanner, J. Robertson, L.M. Brown, Density, sp 3 content and internal layering of DLC films by X-ray reflectivity and electron energy loss spectroscopy, Diam. Relat. Mater. 9 (3) (2000) 771–776.
[5] A. Anders, Approaches to rid cathodic arc plasmas of macro-and nanoparticles: a review, Surf. Coat. Technol. 120 (1999) 319–330.
[6] C.A. Davis, G.A.J. Amaratunga, K.M. Knowles, Growth mechanism and cross-sectional structure of tetrahedral amorphous carbon thin films, Phys. Rev. Lett. 80 (15) (1998) 3280.
[7] M.P. Siegal, et al., Amorphous-tetrahedral diamondlike carbon layered structures resulting from film growth energetics, Appl. Phys. Lett. 73 (6) (1998) 759–761.
[8] A.C. Ferrari, J. Robertson, Resonant Raman spectroscopy of disordered, amorphous, and diamondlike carbon, Phys. Rev. B 64 (7) (2001) 075414.
[9] J. Schwan, S. Ulrich, V. Batori, H. Ehrhardt, S.R.P. Silva, Raman spectroscopy on amorphous carbon films, J. Appl. Phys. 80 (1) (1996) 440–447.
[10] R.N. Tarrant, D.R. McKenzie, M.M.M. Bilek, Raman characterisation of PIII multilayer carbon films, Diam. Relat. Mater. 13 (4) (2004) 1422–1426.
[11] A. Kleiman, A. Márquez, R.L. Boxman, Performance of a magnetic island macroparticle filter in a titanium vacuum arc, Plasma Sources Sci. Technol. 17 (1) (2007) 015008.
[12] M. Fazio, D. Vega, A. Kleiman, D. Colombo, L.F. Arias, A. Márquez, Study of the structure of titanium thin films deposited with a vacuum arc as a function of the thickness, Thin Solid Films 593 (2015) 110–115.
[13] N. Savvides, B. Window, Diamondlike amorphous carbon films prepared by magnetron sputtering of graphite, J. Vac. Sci. Technol. A 3 (6) (1985) 2386–2390.
[14] J.C. Vickerman, D. Briggs, TOF-SIMS Surface Analysis by Mass Spectrometry, first ed. IM Publications and Surface Spectra Limited, 2001.
[15] L. Lianos, C. Quet, T.M. Duc, Surface structural studies of polyethylene, polypropylene and their copolymers with ToFSIMS, Surf. Interface Anal. 21 (1) (1994) 14–22.